

# EAEE4000 Machine learning applications for environmental engineering and sciences

## Using Variational AutoEncoder to understand the spatial features of precipitation response to $CO_2$ increase

Dana Raiter

Instructor: Pierre Gentine

December, 2021

### 1 Introduction

Global mean precipitation is expected to increase by the end of the 21<sub>st</sub> century according to climate models (Collins et al., 2013). These changes can be analyzed in terms of the energy balance of the atmosphere which imply a direct connection between global mean precipitation and temperature changes (Allen and Ingram, 2002; Held and Soden, 2006; O'Gorman et al., 2011).

The response of global mean precipitation to temperature change is defined as the hydrological sensitivity (HS) and is calculated as the slope of precipitation change with surface temperature change (Fläschner et al., 2016). While some studies show that the HS is dependent on the magnitude of  $CO_2$  forcing (Good et al., 2012), due to the energetic constraints on precipitation it is reasonable to assume that the change in the magnitude of  $CO_2$  forcing will not affect the HS, implying a linear connection that is maintained with different  $CO_2$  forcings.

However, The energy balance of the atmosphere is not conserved regionally due to the inhomogeneous response of the atmosphere in different regions. For example, the surface warming over land is much stronger than over the ocean due to the difference in their heat capacity. When examining the regional precipitation change, patterns arise (Xie et al., 2010).

Here, we start by investigating the dependence of the precipitation change on  $CO_2$  by performing a series of abrupt  $CO_2$  model runs using the Community Earth System Model (CESM, Kay et al. (2015)) and calculating the HS for  $2\times$  to  $8\times CO_2$  using a simple linear regression. Then, in order to analyze the precipitation anomaly patterns, we design a Variational AutoEncoder (VAE, Kingma and Welling (2013)) to compress this non-linear data. We compare the VAE to Non-Linear and Linear AutoEncoders. Analyzing results from the VAE model, our goal is to use the latent space (bottleneck) to understand different mechanisms that control the precipitation response patterns.

### 2 Methods

#### Data

We use the fully coupled atmosphere-ocean-sea-ice-land model of CESM and perform a series of abrupt  $CO_2$  forcing runs, with  $1\times$ ,  $2\times$ ,  $3\times$ ,  $4\times$ ,  $5\times$ ,  $6\times$ ,  $7\times$ , and  $8\times CO_2$  forcings, with all other

trace gases, ozone concentrations, and aerosols fixed at PI values. We use the  $1 \times CO_2$  run as a control run and define precipitation change ( $\Delta P$ ) as the difference between runs  $2 - 8 \times CO_2$  and the  $1 \times CO_2$  run. Each run is 150 years long.

## HS- linear regression

We follow Fläschner et al. (2016) and define the hydrological sensitivity parameter as the slope of  $\Delta P$  with  $\Delta T$  (surface temperature change) calculated from linear regression of the two variables:

$$\Delta P = \eta \Delta T + A \quad (1)$$

where  $\eta$  is the HS parameter and A is the fast adjustment of the precipitation to increase of  $CO_2$ .

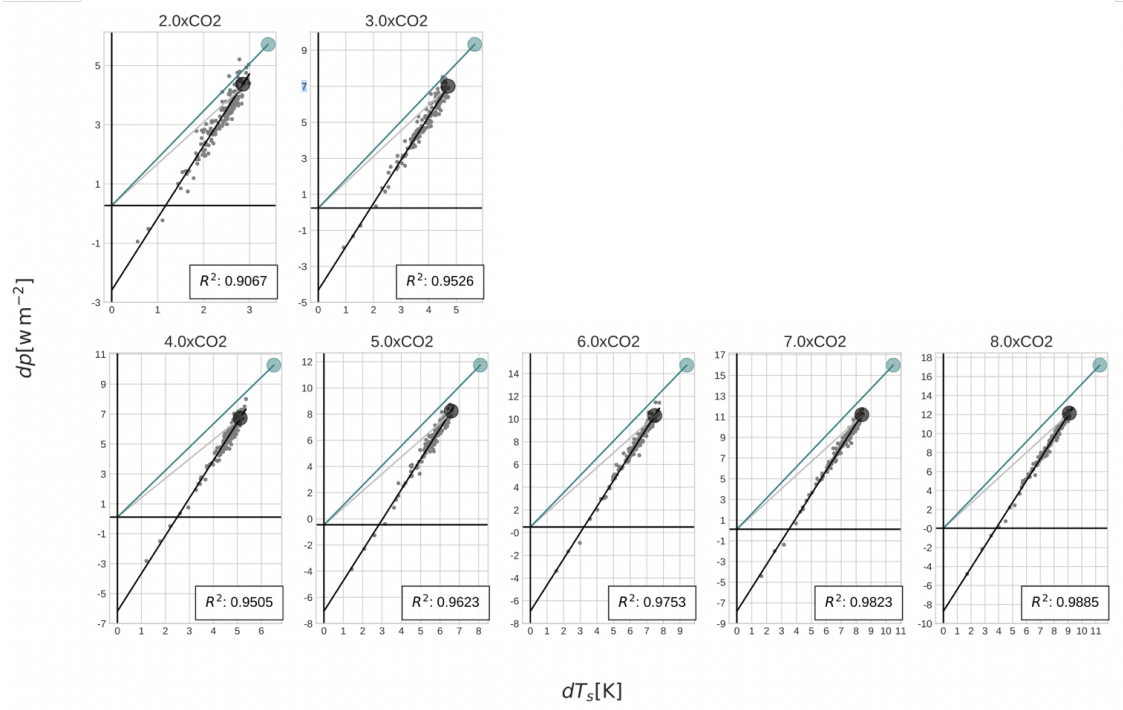


Figure 1: Hydrological sensitivity parameter for  $2 - 8 \times CO_2$ .

Fig. 1 shows the HS parameter calculated for  $2 - 8 \times CO_2$  runs, solid black line is  $\eta$  calculated from linear regression of 150 years of precipitation change and surface temperature change. Gray dots represent the data. We can easily see that the linear regression fits the data very well, and indeed we see a linear relationship between the global mean precipitation and surface temperature changes. Our goal is to understand the patterns of regional precipitation change, and therefore use a more sophisticated method— machine learning.

## Machine learning methods

We start by creating 3 different models, following a similar architecture: Variational AutoEncoder (VAE), Non-linear AutoEncoder (NLAE) and a Linear AutoEncoder (LAE). All models use an encoder which receives as input the precipitation change map (Fig. 3), with size 192x288. We then have 3 hidden layers reducing the input size to a latent space of 2 or 4 nodes. The VAE and NLAE

models use ReLu as the activation function for the first layers and a linear activation for the last. The LAE uses a linear activation function for all layers. In the VAE model, we calculate  $\mu$  and  $\sigma$  in the latent space and use them to reparameterize  $z$ , the lower dimensional representation of the input data, the output of the encoder.

Table 1: Hyperparameter values

Hyperparameter	Value
Training epochs	100
Batch size	4
Latent space dim	2/4
KL weight	0.8

We pair this encoder with a decoder, with the same, but opposite architecture to expand the latent space back to a map of the original size. In the NLAE and LAE we use a standard MSE function to calculate loss. In the VAE, however, we use a loss function comprised of an MSE component and a weighted KL divergence component. Hyperparameters values are shown below in Table 1. We train all models with the first 90 years of each data set, and test with the last 60 years.

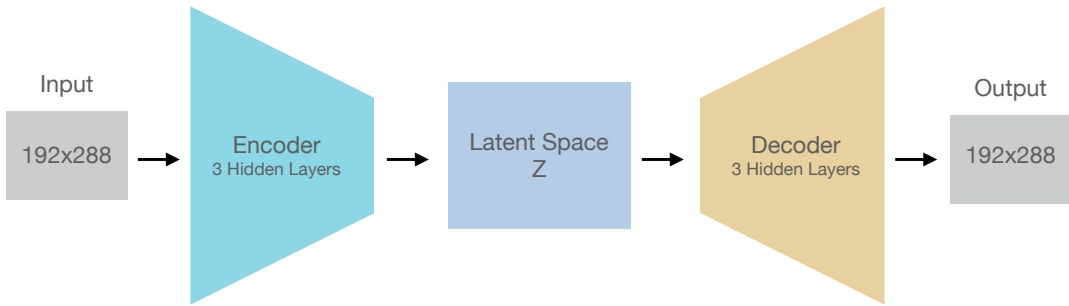


Figure 2: Model architecture.

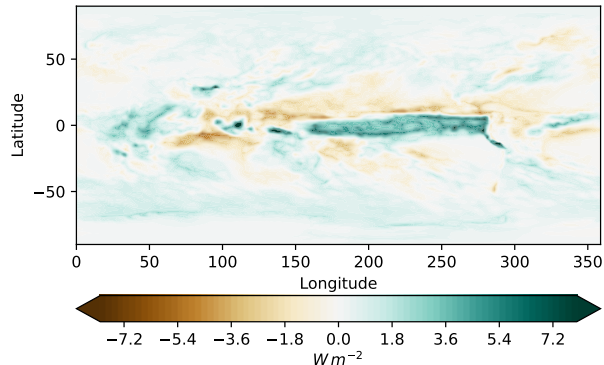


Figure 3: Example of input. Precipitation change map from  $4 \times CO_2$  run, with size 192x288. Units are  $W m^{-2}$

### 3 Results and Analysis

Fig. 4 shows an example of reconstruction of the input in Fig. 3, using all three models and their losses. There are differences between the three and as expected, the VAE performs slightly better, hence, all further analysis will be based on the VAE. It is important to remember that the loss function of VAE consists of two loss functions and by definition will have larger values than the MSE loss alone. In addition, we believe that with adequate amount of training data and epochs the VAE will outperform the other two models.

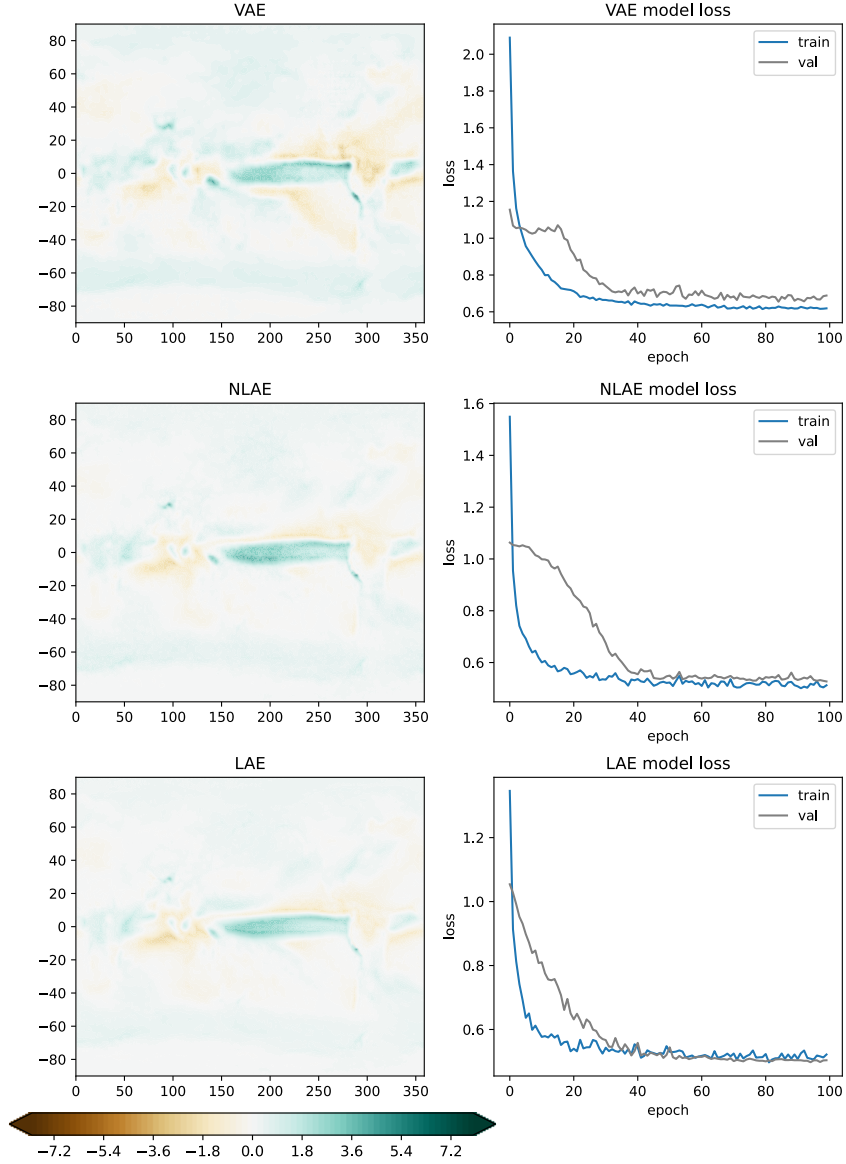


Figure 4: Examples of reconstruction using the VAE, NLAE and LAE and their losses.

#### Analyzing the latent space

In order to analyze the patterns of precipitation change, we investigate the latent space, since it holds information about components of said patterns. By visualizing the different nodes of the latent

space, we aim to identify different drivers and modes of variability of the precipitation change. We run the test data through the encoder and analyze the results of each node in the latent space. We performed this calculation for latent spaces with 2 and 4 dimensions. Fig. 5 and 6 show the distribution of the each node in  $z$ .

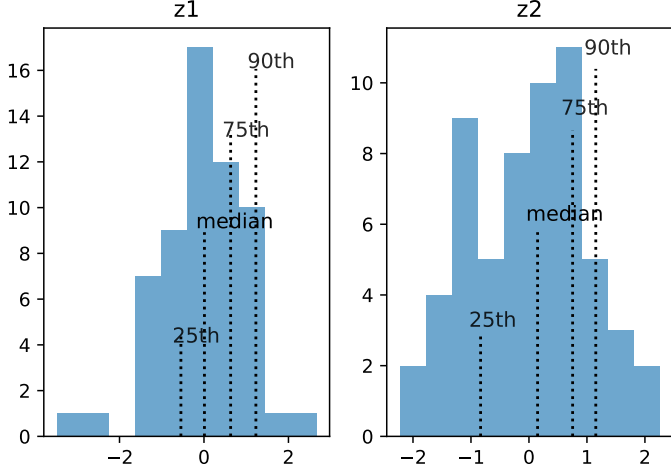


Figure 5: Latent space nodes distribution and percentiles for latent space width=2.

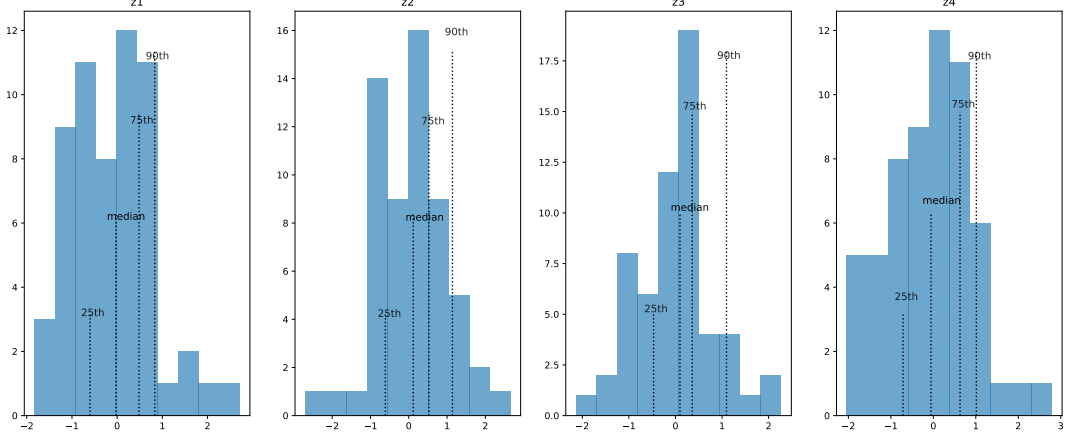


Figure 6: Latent space nodes distribution and percentiles for latent space width=4.

We reconstruct the precipitation change map using the median values of each node of  $z$ , and feeding it into the decoder. Fig. 7 presents the median reconstruction for all 7 data sets ( $2 \times -8 \times CO_2$ ), for simplicity, here we will show only an example of  $4 \times CO_2$  data set analysis.

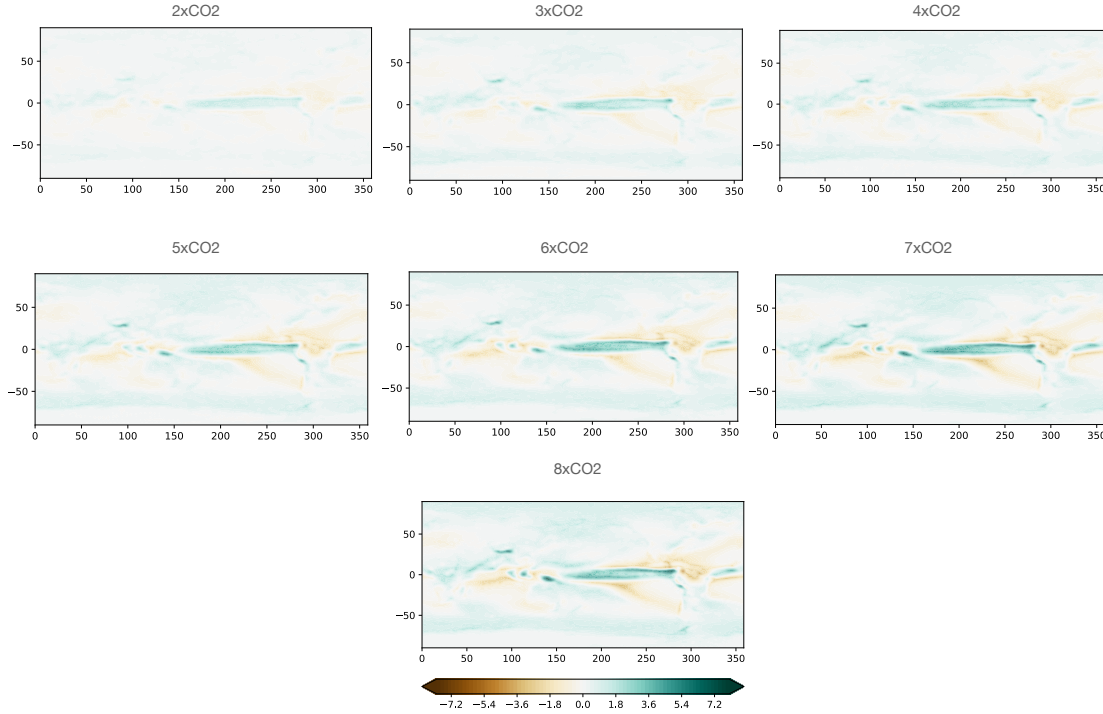


Figure 7: Reconstruction of precipitation change map using the median values of  $z$ .

To understand the modes of variability, we reconstruct the precipitation change maps using different percentiles of a single node and the median for the remaining nodes, e.g.,  $z = [z_{125th}, z_{2median}, z_{3median}, z_{4median}]$ . We hope that by observing these results we could identify distinct physical processes. We perturbed each node between the 25<sup>th</sup> and 90<sup>th</sup> percentiles and calculate the difference between the two (Fig. 8, 9).

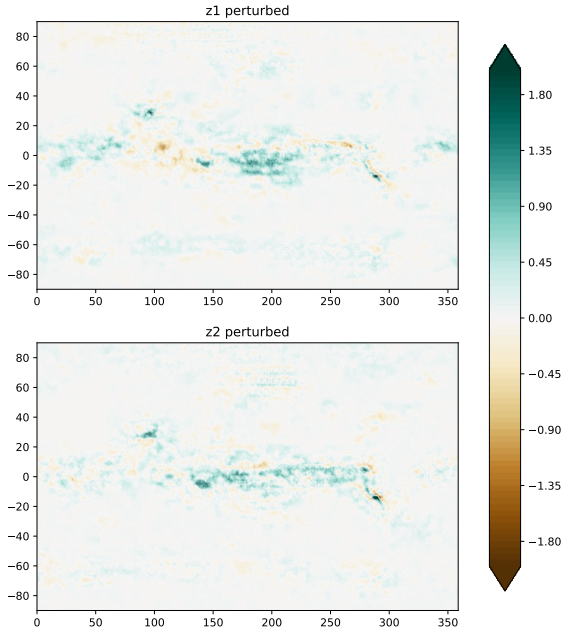


Figure 8: Difference of reconstructed precipitation change maps of each perturbed node of  $z$  for latent space width 2.

The perturbed results are quite noisy, likely due to the low amount of training and test data, and it is therefore difficult to draw decisive conclusions. With that, when choosing the latent width to be 2, two patterns arise (Fig. 8) that can be somewhat interpreted as dynamic and thermodynamic processes which are known to be the controlling processes of precipitation changes in the tropics (Seager et al., 2010). The thermodynamic processes describe changes in precipitation as a result of increase of water vapor due to global warming, in our case induced by increasing  $CO_2$ , therefore, change in a node explaining these mechanisms should highlight the ITCZ region where convection occurs. The dynamic processes drive changes in precipitation as a result of the large-scale circulation change and therefore, perturbing a node explaining these mechanisms can vary with longitude, showing changes in the zonal circulation.

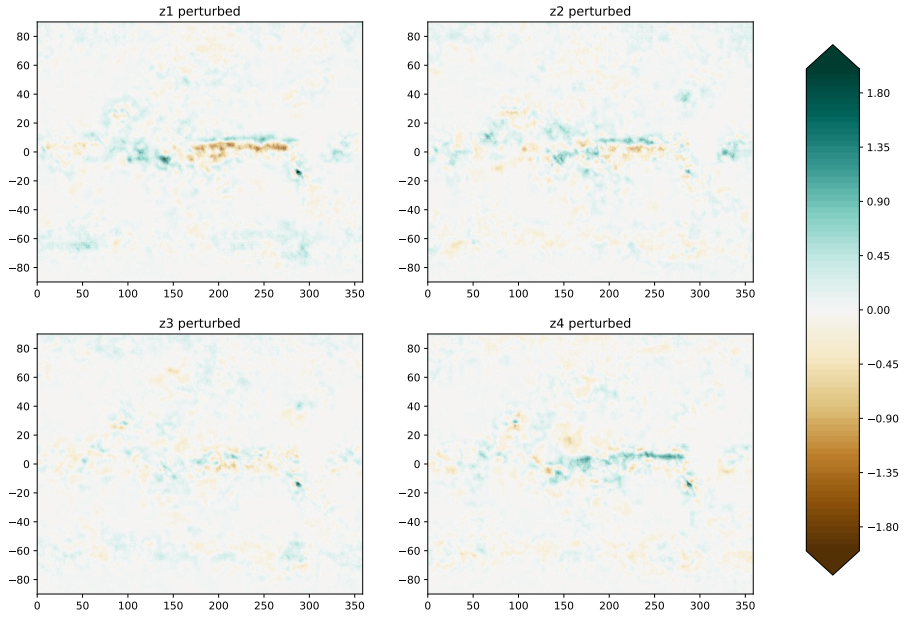


Figure 9: Difference of reconstructed precipitation change maps of each perturbed node of  $z$  for latent space width 4.

## 4 Summary and discussion

We started this project by analyzing the HS for model runs with different magnitude of  $CO_2$  forcing. It is very clear that fitting the global mean precipitation change using linear regression works very well. This motivated us to further investigate the precipitation change by observing the regional changes, i.e, without globally averaging. Since the atmosphere's energy budget is not conserved in specific regions, we turned to machine learning methods to try to understand patterns of the precipitation changes.

We compared three models (VAE, NLAE and LAE) and showed that the most accurate reconstruction results from using the VAE model. Then, we analyze the latent space nodes to identify physical mechanisms driving the precipitation change. The main shortcoming of our analysis is the small amount of data, which caused noisy and inconclusive results. In addition, for the sake of this analysis, and a simpler presentation of the project, we only show results from the  $4 \times CO_2$  model run. A next step for the future could be to compare the latent space nodes across different forcings and to identify how the precipitation change mechanisms are dependent on the magnitude of  $CO_2$ .

Following this course, we can take the architecture designed here and apply it to other data sets, for example, data form CMIP6 which we know contains many model runs and a more fitting amount of data.

## References

- Allen, M. R. and Ingram, W. J. (2002). Constraints on future changes in climate and the hydrologic cycle. *Nature*, 419(6903):228–232.
- Collins, M., Knutti, R., Arblaster, J., Dufresne, J.-L., Fichefet, T., Friedlingstein, P., Gao, X., Gutowski, W., Johns, T., Krinner, G., Shongwe, M., Tebaldi, C., Weaver, A., and Wehner, M. (2013). *Long-term Climate Change: Projections, Commitments and Irreversibility*, book section 12, page 1029?1136. Cambridge University Press.
- Flaschner, D., Mauritsen, T., and Stevens, B. (2016). Understanding the intermodel spread in global-mean hydrological sensitivity. *J. Climate*, 29(2):801–817.
- Good, P., Ingram, W., Lambert, F. H., Lowe, J. A., Gregory, J. M., Webb, M. J., Ringer, M. A., and Wu, P. (2012). A step-response approach for predicting and understanding non-linear precipitation changes. *Clim. Dyn.*, 39(12):2789–2803.
- Held, I. M. and Soden, B. J. (2006). Robust responses of the hydrological cycle to global warming. *Journal of Climate*, 19(21):5686–5699.
- Kay, J. E., Deser, C., Phillips, A., Mai, A., Hannay, C., Strand, G., Arblaster, J. M., Bates, S. C., Danabasoglu, G., Edwards, J., Holland, M., Kushner, P., Lamarque, J.-F., Lawrence, D., Lindsay, K., Middleton, A., Munoz, E., Neale, R., Oleson, K., Polvani, L., and Vertenstein, M. (2015). The community earth system model (CESM) large ensemble project: A community resource for studying climate change in the presence of internal climate variability. *Bulletin of the American Meteorological Society*, 96(8):1333–1349.
- Kingma, D. P. and Welling, M. (2013). Auto-encoding variational bayes.
- O’Gorman, P. A., Allan, R. P., Byrne, M. P., and Previdi, M. (2011). Energetic constraints on precipitation under climate change. *Surveys in Geophysics*, 33(3-4):585–608.
- Seager, R., Naik, N., and Vecchi, G. A. (2010). Thermodynamic and dynamic mechanisms for large-scale changes in the hydrological cycle in response to global warming\*. *Journal of Climate*, 23(17) : 4651 – –4668.
- Xie, S.-P., Deser, C., Vecchi, G. A., Ma, J., Teng, H., and Wittenberg, A. T. (2010). Global warming pattern formation: Sea surface temperature and rainfall. *J. Climate*, 23(4):966–986.